Quantum Fluctuations in the Fröhlich Condensate of Molecular Vibrations Driven Far From Equilibrium

Zhedong Zhang,[1,*] Girish S. Agarwal,[1,†] and Marlan O. Scully[1,2,3,‡]
[1]Texas A&M University, College Station, Texas 77843, USA
[2]Baylor University, Waco, Texas 76704, USA
[3]Princeton University, Princeton, New Jersey 08544, USA

(Received 18 October 2018; revised manuscript received 7 March 2019; published 19 April 2019)

Fröhlich discovered the remarkable condensation of polar vibrations into the lowest frequency mode when the system is pumped externally. For a full understanding of the Fröhlich condensate one needs to go beyond the mean field level to describe critical behavior as well as quantum fluctuations. The energy redistribution among vibrational modes with nonlinearity included is shown to be essential for realizing the condensate and the phonon-number distribution, revealing the transition from quasithermal to super-Poissonian statistics with the pump. We further study the spectroscopic properties of the Fröhlich condensate, which are especially revealed by the narrow linewidth. This gives the long-lived coherence and the collective motion of the condensate. Finally, we show that the proteins such as bovine serum albumin and lysozyme are most likely the candidates for observing such collective modes in THz regime by means of Raman or infrared spectroscopy.

DOI: 10.1103/PhysRevLett.122.158101

Introduction.—The collective properties in both physical and biological systems attracted attention during the past decades and are of importance for understanding many peculiar phenomena, such as the phase transition of polaritons [1–3], superefficient energy transfer in photosynthesis [4–7], and cognitive function of some molecular machinery at work in living cells [8,9]. The latter possibly stems from the collective oscillations of biomolecules, making giant dipole moments that activate long-range electric forces. To understand these, Fröhlich suggested a condensation of energy at the lowest mode of polar vibrations once the external energy supply exceeds a threshold [10], and this idea was further followed by others for detailed investigation over three decades [11–14]. Provided the sufficient energy pump, this large accumulation of phonons considerably builds up at the lowest mode. Though this seems a reminiscence of Bose-Einstein condensate (BEC) [15–18], but in detail the Fröhlich condensate is more like a laser. We note however the close relation between the quantum theory of laser and a BEC [19–23]. Recent simulations based on Wu-Austin Hamiltonian specified the parameter regime for weak, mediate, and strong condensates in various proteins [24,25].

To achieve such out-of-equilibrium condensate, the energy redistribution essentially plays an important role in introducing the nonlinearity [10,25,26]. The emergence of Fröhlich condensate is analogous to laser operation [23,27], which offers new insight to understand the cooperative phenomena in various systems [28,29]. The coherent nature of laser is manifested by narrow linewidth. Thereby, under proper conditions the Fröhlich condensate would show the coherent feature which is one of the main tasks of this work.

The combination of recent advance on x-ray crystallography [30] and THz radiation offers effective tools for visualizing the structural change associated with low-frequency collective vibrations in the materials, i.e., lysozyme protein crystals [31,32]. The structural change has been observed to sustain for micro- to milliseconds, which is several orders of the magnitude longer than the one induced by the redistribution of THz vibrations toward thermal distribution [31]. It seems plausible to attribute this phenomena to Fröhlich condensate that causes nonthermal distribution. The most recent experiment demonstrated in bovine serum albumin (BSA) protein the remarkable absorption feature around 0.314 THz, when driving the system by optical pumping [33]. Understanding these interesting and intriguing experiments will lead us to the deeper understanding of Fröhlich's mechanism, because the cooperativity has been shown to exist in some non-physical systems [34,35]. On the other hand, this out-of-equilibrium cooperativity manifests itself even at classical level, e.g., the long-survived limit cycle oscillation in gene network [36,37]. Thus, it is important to obtain a detailed understanding of the coherence of the Fröhlich condensate, which is still obscure, especially in THz regime. Clearly a full understanding can come solely from a quantum theory which would give not only the mean but also quantum fluctuations as well as linewidth information, crucial in spectroscopic measurement.

In this Letter, we develop a full quantum statistical theory for Fröhlich condensate. We analytically find that the phonon-number distribution evolves with external

energy pump, from quasithermal to the statistics found in Scully-Lamb theory of the laser [19,20]. Besides, the long-lived coherence of the condensate is observed, i.e., the dramatic increase of the lifetime by ∼10 times for BSA under room temperature (∼50 times under low temperature). This subsequently characterizes the narrow linewidth in the spectroscopic signal. We suggest some possible candidates for observing the Fröhlich condensate, such as lysozyme and BSA proteins rather than the longitudinal vibrations of microtubules. Moreover, the phonon statistics paves the road for evaluating the quantum fluctuations in the condensate particles, which have been reported in recent experiments on exciton polaritons [38].

Model and equation of motion.—For the low-frequency vibrations in molecules, i.e., THz intramolecular vibrations of proteins and low-energy phonon modes in DNA, the surrounding medium (like solvent or water) acts as a thermal environment, resulting in the energy dissipation and redistribution. The latter shows the nonlinearity which is substantial in biological functions involving the low-loss energy transport through protein in DNA [39]. Besides, these vibrational modes are excited by a continuous energy supply, shown in Fig. 1. We may model the system as a group of harmonic oscillators with the frequency spectrum ω_j, $(j = 0, 1, 2, \ldots, D)$ where $D \gg 1$ denotes the total number of vibrational modes. The effect

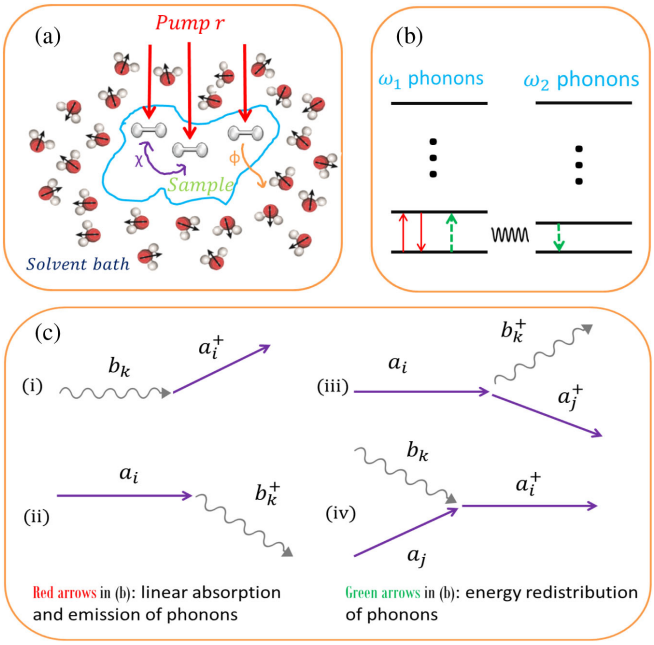

FIG. 1. (a) Schematic of molecular vibrations driven into far-from-equilibrium regime; (b) Vibrational modes absorb energy from external source at rate of r and surrounding medium acting as thermal bath causes the dissipation at rate of ϕ, corresponding to the 1st term in Eq. (1). Bath is also responsible for the energy redistribution (nonlinear) at rate of χ, corresponding to the 2nd term in Eq. (1); (c) Feynman diagrams for those 1st and 2nd order processes.

of external pump and environment is governed by the coupling $V(t) = V_p(t) + [V_{\rm env}(t) + \text{H.c.}]$, where $V_p(t) = \sum_{s=0}^{D} [F_s^*(t) a_s e^{-i\omega_s t} + \text{H.c.}]$ and

$$V_{\rm env}(t) = \sum_k \left(\sum_{s=0}^{D} \frac{f_{s,k}}{\sqrt{2}} a_s^\dagger b_k e^{i\Delta_s^k t} + \sum_{s>l\geq 0}^{D} \frac{G_{sl,k}}{\sqrt{2}} a_s^\dagger a_l b_k e^{i\Delta_{sl}^k t} \right). \tag{1}$$

The pumping field is characterized by a broad spectrum $\langle F_s(t) F_l^*(t')\rangle = (r/2)\delta_{sl}\delta(t-t')$ with a pumping rate of r, $\Delta_{sl}^k = \omega_s - \omega_l - v_k$, and $\Delta_s^k = \omega_s - v_k$. a_s and b_k stand for the bosonic annihilation operators for molecular vibrations and bath modes, respectively. The first term in Eq. (1) describes the energy exchange between the vibrational modes and environment, giving the dissipation (one-phonon process). The second term in Eq. (1) quantifies the two-phonon process, causing energy redistribution between the vibrational modes [24]. Defining the density matrix $\rho_{n_0,m_0} = \sum_{\{n_l\}} \langle n_0; \{n_l\}|\rho|m_0; \{n_l\}\rangle$ for the mode ω_0, the equation of motion may be derived [23,40,41], and all the details are given in the Supplemental Material [42]. The full master equation results in the equation which the total phonon number $N = \sum_{s=0}^{D} \langle a_s^\dagger a_s \rangle$ obeys: $\dot{N} = (D+1)(r + \phi\bar{n}) - \phi N$ showing that the total phonon number is *solely* dictated by the external pumping and dissipation. r and $\phi = 2\pi f_\omega^2 \mathcal{D}(\omega)$ refer to the rates of energy pumping and dissipation, respectively. $\bar{n} = [\exp(\hbar\omega_0/k_B T) - 1]^{-1}$ is the Planck factor. Thus, N does not depend on the processes (iii) and (iv) in Fig. 1(c). We can then replace N by its stationary value as the timescale of interest $t > \phi^{-1}$. Thereby, N can be partitioned into $N = N_r + N_{\rm th}$, where $N_r = (D+1)r/\phi$ and $N_{\rm th} = (D+1)\bar{n}$. This manifests the contributions to the total excitation from external pumping r and thermal distribution $\bar{n}$. Such observation enables us to derive a simple equation for the population at the lowest vibrational mode ω_0, assuming $\langle n_0 N\rangle \simeq \langle n_0\rangle N$.

$$\begin{aligned}\dot{\rho}_{n_0,n_0} = &-(r + \phi\bar{n} + \chi\mathcal{N}_{n_0})(n_0+1)\rho_{n_0,n_0} \\ &+ (r + \phi\bar{n} + \chi\mathcal{N}_{n_0-1}) n_0 \rho_{n_0-1,n_0-1} \\ &- [r + \phi(\bar{n}+1) + \chi\mathcal{M}_{n_0}] n_0 \rho_{n_0,n_0} \\ &+ [r + \phi(\bar{n}+1) + \chi\mathcal{M}_{n_0+1}](n_0+1)\rho_{n_0+1,n_0+1},\end{aligned} \tag{2}$$

from the reduced master equation, where $\chi = 2\pi G_\omega^2 \mathcal{D}(\omega)$ refers to the rate of energy redistribution $\mathcal{N}_{n_0} = \sum_{j=1}^{D} (\bar{n}_{\omega_{j0}} + 1)\langle n_j\rangle_{n_0}$, $\mathcal{M}_{n_0} = \sum_{j=1}^{D} \bar{n}_{\omega_{j0}} \langle n_j + 1\rangle_{n_0}$. There are varying degrees of rigor to evaluate $\mathcal{N}_{n_0}$ and $\mathcal{M}_{n_0}$. We will choose the one assuming $\bar{n}_{\omega_{j0}} \simeq \bar{n}$ which leads to $\mathcal{N}_{n_0} \simeq (\bar{n}+1)(N - n_0)$, $\mathcal{M}_{n_0} \simeq \bar{n}(N - n_0 + D)$. Equation (2) has a nice interpretation in terms of the probability flows as depicted in Fig. 2.

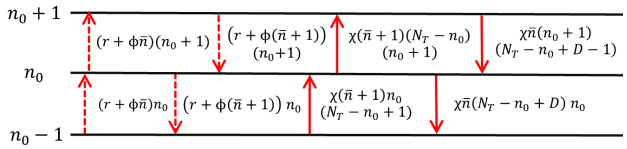

FIG. 2. Transition diagram in accordance to Eq. (2), showing the flow of probability in and out of the $|n_0\rangle$ state from and to the neighboring $|n_0+1\rangle$ and $|n_0-1\rangle$ states. $(r+\phi\bar{n})(n_0+1)$ and $(r+\phi(\bar{n}+1))(n_0+1)$ represent the respective phonon emission and absorption, due to the one-phonon processes (pumping and dissipation); $\chi(\bar{n}+1)(N_T-n_0)(n_0+1)=\phi\bar{n}(n_0+1)(\chi(\bar{n}+1)/\phi\bar{n})(N_T-n_0)$ corresponds to the process in which phonons are emitted owing to both dissipation and energy redistribution; $\chi\bar{n}(N_T-n_0+D-1)(n_0+1)=\phi(\bar{n}+1)(n_0+1)[\chi\bar{n}/\phi(\bar{n}+1)]\times(N_T-n_0+D-1)$ corresponds to the process in which phonons are absorbed owing to both dissipation and energy redistribution. Similar explanations exist for the other terms.

Out-of-equilibrium condensation of phonons.—To illustrate the condensation of phonons and their critical behaviors, we essentially obtain the rate equation for phonon number $\langle n_0\rangle$ at the lowest mode

$$\langle\dot{n}_0\rangle=(\chi N_r-\phi-\chi)\langle n_0\rangle-\chi\langle n_0^2\rangle+[r+\phi\bar{n}+\chi(\bar{n}+1)N]. \tag{3}$$

The mode ω_0 experiences gain due to the pumping of all the modes and loses energy via the terms $(\phi+\chi)\langle n_0\rangle$ as well as $\chi\langle n_0^2\rangle$. The last bracket in Eq. (3) leads to the residue number of phonons in mode ω_0 even below the pumping threshold

$$r_c=\frac{\phi}{D+1}\left(1+\frac{\phi}{\chi}\right), \tag{4}$$

as indicated by $\chi N_r-(\phi+\chi)>0$ in Eq. (3). The equation for $\langle n_0\rangle$ has a structure which is a reminiscence of the photon number for a single mode laser.

Further simplification neglects the fluctuation of n_0, namely, $\langle n_0^2\rangle\simeq\langle n_0\rangle^2$, which gives the steady-state phonon number at mode ω_0 shown in Fig. 3(a) where the parameters are taken from recent experiment [33].

Coherence of condensate and linewidth.—As a collective mode, the in-phase motion should be maintained in the condensate. This is featured by the long-lived or long-range coherence, which may be deeply connected to the so-called off-diagonal long-range order in superconductivity and superfluidity [43]. The coherence of our condensate is quantified by the off-diagonal elements of density matrix ρ_{n_0,n_0+1}. To probe such coherence properties, we can use infrared or Raman spectroscopies. From the reduced master equation, the coherence dynamics obeys

$$\begin{aligned}\dot{\rho}_{n_0,n_0+1}=&(i\omega_0-\gamma_{n_0})\rho_{n_0,n_0+1}+c_{n_0-1}\rho_{n_0-1,n_0}\\&-(c_{n_0}+d_{n_0})\rho_{n_0,n_0+1}+d_{n_0+1}\rho_{n_0+1,n_0+2},\end{aligned} \tag{5}$$

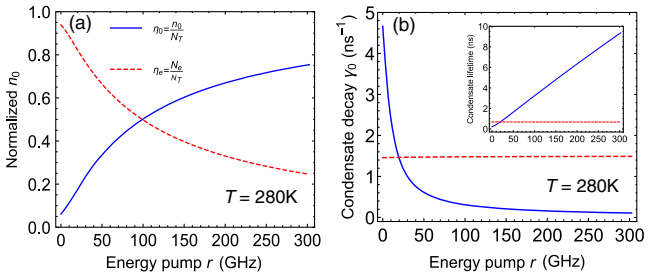

FIG. 3. (a) Phonon numbers at the lowest mode ω_0 and excited modes $\omega_l(l\geq 1)$ normalized by total phonon number N vary with external energy supply. (b) Damping rate γ_0 of condensate varies with external energy supply. Lifetime $1/\gamma_0$ is plotted in small panel. In (b), dashed red line is for the case with no Fröhlich condensate when turning off the nonlinearity. Solvent temperatures $T=280$ K, corresponding to $\bar{n}=16$. Parameters are taken from Ref. [33] for BSA protein: $\omega_0=0.314\times 2\pi$ THz, $\phi=6$ GHz, $\chi=0.07$ GHz, and $D=200$.

where

$$\gamma_{n_0}=\frac{1}{4}\left(\frac{r+\phi(\bar{n}+1)+\chi\bar{n}(N-n_0+D)}{\sqrt{n_0(n_0+1)}+n_0+\frac{1}{2}}+\frac{r+\phi\bar{n}+\chi(\bar{n}+1)(N-n_0)}{\sqrt{(n_0+1)(n_0+2)}+n_0+\frac{3}{2}}\right), \tag{6}$$

and $c_{n_0}=\sqrt{(n_0+1)(n_0+2)}[r+\phi\bar{n}+\chi(\bar{n}+1)(N-n_0)]$, $d_{n_0}=\sqrt{n_0(n_0+1)}[r+\phi(\bar{n}+1)+\chi\bar{n}(N-n_0+D)]$. To solve Eq. (5), we have the ansatz $\rho_{n_0,n_0+1}(t)=\exp[i\omega_0 t-D_{n_0}(t)]\rho_{0,1}(0)\prod_{m=1}^{n_0}c_{m-1}/d_m$ by imposing the detailed balance into the initial condition $c_{n_0}\rho_{n_0,n_0+1}(0)=d_{n_0+1}\rho_{n_0+1,n_0+2}(0)$ [41]. The slow variation of γ_{n_0} with respect to t gives $|D_{n_0-1}-D_{n_0}|\ll 1$ yielding $D_{n_0}(t)\simeq\gamma_{n_0}t$. We can thereby safely replace n_0 in γ_{n_0} by $\langle n_0\rangle$. Hence, the vibrational coherence of the lowest mode is approximated to $\rho_{n_0,n_0+1}(t)\propto e^{(i\omega_0-\gamma_0)t}$ where the lifetime is given by

$$\gamma_0\simeq\frac{r+\phi(\bar{n}+\frac{1}{2})}{4\langle n_0\rangle}, \tag{7}$$

for the energy supply much above threshold. Equation (7) elucidates the considerable suppression of the damping rate by large condensation of phonons. This is further supported by the numerical calculations displayed in Fig. 3(b). It shows that the coherence lifetime when driving system into far-from-equilibrium regime ($r\simeq 200$ GHz) is ~10 times than the expected one induced by the redistribution of THz vibrations toward thermal distribution. This, in other words, will result in a remarkably sharp peak in the infrared and Raman spectroscopies.

From the standard definition, we find the infrared fluorescence spectra governed by $\langle\mu^{(+)}(t)\mu^{(-)}(0)\rangle$ where $+(-)$ denotes the raising (lowering) part of the dipole operator

$$S_{\mathrm{FL}}(\omega)=\frac{32\pi^2 M\omega}{3\hbar\Omega}\sum_{j=0}^{D}\frac{|\mu_j|^2\gamma_j\langle n_j\rangle}{(\omega_j-\omega)^2+\gamma_j^2}, \tag{8}$$

where γ_j^{-1} stands for the lifetime of the jth vibrational mode. $|\mu_j|$ refers to the magnitude of electric dipole moment of the jth mode. Ω is the bulk volume and M stands for the amount of molecules. The $j=0$ term in Eq. (8) shows a high-intensity peak and a narrow linewidth associated with Fröhlich condensate as supported by Fig. 3(b).

Phonon statistics of Fröhlich condensate.—To gain more information about the out-of-equilibrium condensate of phonons obtained above, we proceed via the fluctuations of phonon number which is governed by the phonon distribution

$$P(n_0)=P(0)\left(\frac{\alpha}{\beta}\right)^{n_0}\frac{\Gamma(\frac{\mathcal{X}}{\alpha})\Gamma(\frac{\mathcal{Y}}{\beta}-n_0)}{\Gamma(\frac{\mathcal{X}}{\alpha}-n_0)\Gamma(\frac{\mathcal{Y}}{\beta})}, \tag{9}$$

at steady state where $P(n_0)\equiv\rho^{ss}_{n_0,n_0}$. $\mathcal{X}=r+\phi\bar{n}+\chi(\bar{n}+1)(N+1)$, $\mathcal{Y}=r+\phi(\bar{n}+1)+\chi\bar{n}(N+D)$ and $\alpha=\chi(\bar{n}+1)$, $\beta=\chi\bar{n}$. The nonmonotonic feature of phonon distribution appears when $n_{\mathrm{cr}}\geq 1$ such that $P(n_0)>P(n_0-1)$ as $n_0<n_{\mathrm{cr}}$ while $P(n_0)<P(n_0-1)$ as $n_0>n_{\mathrm{cr}}$, where $n_{\mathrm{cr}}=N+1-(\phi/\chi)-\bar{n}D$. The condition $n_{\mathrm{cr}}\geq 1$ implies a threshold of energy supply, which coincides with the one predicted by Eq. (4) when $D\gg 1$. Hence, we can evidently conclude that the out-of-equilibrium condensate is featured by the nonthermal distribution of phonons, showing an analogy to the photon number statistics for a single mode laser rather than the atomic BEC [23,41].

In terms of $P(n_0)$ given by Eq. (9), we are able to obtain the fluctuation of n_0 in further and the higher moments $\langle n_0^{\ell}\rangle$ will be presented elsewhere. For the energy pump appreciably above threshold, we have the condensate ratio defined as $\eta=\langle n_0\rangle/N$ and Mandel parameter $Q=\langle\Delta n_0^2\rangle/\langle n_0\rangle-1$

$$\eta=1-\frac{\phi(\phi+\chi\bar{n}D)}{\chi(D+1)(r+\phi\bar{n})}$$
$$Q=\frac{(r+\phi\bar{n})[\phi-\chi(D+1)]+\phi(\bar{n}+2)(\phi+\chi\bar{n}D)}{\chi(D+1)r+\phi(\chi\bar{n}-\phi)}. \tag{10}$$

Increasing the external energy pump, Q will become negative as long as $(\chi/\phi)>(1/D+1)$, so that sub-Poissonian distribution of phonons will show up, manifesting the nonclassical properties. This is supported by the numerical calculations of phonon statistics shown in the Supplemental Material [42].

Figure 4 illustrates the phonon statistics of the lowest vibrational mode ω_0 of BSA protein at room temperature, with respect to various rates of energy supply. The

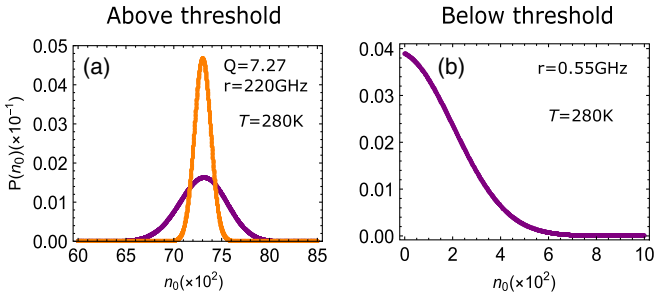

FIG. 4. Phonon distribution of the lowest vibrational mode where the solvent temperature is $T=280$ K corresponding to $\bar{n}=16$. Energy pump (a) $r=220$ GHz, (b) $r=0.55$ GHz; orange dots correspond to Poissonian distribution. Other parameters are the same as that in Fig. 3.

super-Poissonian distribution is shown in Fig. 4(a) with the condensate ratio $\langle n_0\rangle/N\simeq 69\%$, when protein is pumped at the rate of $r\simeq 220$ GHz above the threshold. This would be feasible because the energy pump is still not strong compared to the vibrational frequencies ~0.3 THz of BSA protein. However, the threshold for sub-Poissonian statistics is estimated to be $r=2.98$ THz, which considerably exceeds its vibrational frequencies ~0.3 THz. This indicates a strong-field pump that would however cause other effects, such as anharmonicity and ionization. Hence, the observation of condensate of phonons at the lowest mode would be feasible under room temperature, but the nonclassical distribution will be smeared out. This is more feasible when cooling the surround medium, which is shown in Fig. S1 of the Supplemental Material [42].

It should be noted that the quantum fluctuations beyond the mean field treatment raised much attention in atomic BEC thanks to the experimental advance during last two decades [17]. The large fluctuations especially in the vicinity of critical point often makes the mean-field theory breakdown, but is crucial for understanding the critical phenomenon, e.g., superfluid-insulator transition. The phonon-number fluctuation in Fröhlich condensate would become experimentally accessible by measuring the statistics of photons scattered by the condensate. The photon statistics can be then reconstructed and has been demonstrated in recent experiments on different system, e.g., exciton polaritons [38].

Discussion and conclusion.—To experimentally implement the Fröhlich condensate, many systems were suggested, i.e., microtubules [44–47], BSA, and lysozyme proteins [31–33] as the most favorite ones. But the feasibility of these samples is still in debate. First let us see BSA protein with the size $140\,\mathring{\mathrm{A}}\times 40\,\mathring{\mathrm{A}}\times 40\,\mathring{\mathrm{A}}$. The area that the sub-THz laser with the wavelength $\lambda\simeq 400\ \mu$m focuses on the sample is taken as $A\simeq\lambda^2/4\simeq 40\,000\ \mu\mathrm{m}^2$, in accordance to the diffraction limit. Using the parameters for Fig. 3, our quantum theory leads to the

estimation of energy supply to produce the condensate ratio of 50%: $P_\omega \simeq r\hbar\omega_0 \simeq 20$ pW given by $r \simeq 101$ GHz. With the cross section of light scattering for resonance absorption $\sigma \sim 10^{-15}$ cm^2, we proceed via the number of photons captured by protein molecules $N = A/\sigma \sim 4 \times 10^{11}$, which yields the laser power $P \simeq P_\omega N \sim 8$ W. This would be feasible for the recent development of high-power laser using frequency mixing [48].

To overcome the difficulty of using very strong laser power is to induce the optical excitations of some fluorochromes (i.e., Alexa488) covalently bound to each protein molecule [33]. The excited fluorochromes create fluorescence, resulting in the transfer of some residue energy into the vibrational modes of protein. In practice, this method takes the advantage of avoiding the optical transition of protein and suppressing the absorption by surrounded water molecules which causes the laser-induced heating up, when pumped by the Argon laser with wavelength of 488 nm. Also, such indirect pumping scheme would demand much less laser power than the one using infrared laser, due to the fact that the smaller laser spot can be achieved in optical regime. For creating the condensate with ratio of 80% in BSA, the Argon laser power is estimated to be ≃155 mW within the focusing area 10×10 μm.

For lysozyme protein, the recent advances in both experiments and theory found the sub-THz excitation at $\omega_0 = 0.4 \times 2\pi$ THz and the damping rate $\phi \sim 1$ GHz [31,49]. Because of the diffraction limit, the area that the sub-THz laser with the wavelength $\lambda \simeq 400$ μm focuses on the sample is taken as $A \simeq \lambda^2/4 \simeq 40\,000$ μm^2. Under the room temperature, the full quantum theory estimates the energy supply for the condensate ratio of 50%: $P_\omega \simeq 4.2$ pW given by $r \simeq 16$ GHz. Then the number of photons captured by the sample reads $N = A/\sigma \sim 4 \times 10^{11}$, yielding the laser power $P \simeq P_\omega N \sim 1.6$ W. This would be feasible for cw THz laser [48].

In conclusion, we have developed a full quantum statistical theory using nonequilibrium equations of motion for the Fröhlich condensate. Our model goes beyond the precedent results by providing a description of the critical behavior of the phase transition toward the condensation of phonons. Furthermore, the model led us to the phonon-number distribution of the condensate with the energy pumping, evolving from quasithermal to laser statistics. This yields an analogy to laser operation. Moreover, the long-lived coherence as manifested allows the experimental probe of such collective mode, evident by the remarkably sharp peak with *narrow* linewidth, as in a laser. The development of quantum statistical theory for Fröhlich condensate, especially the fluctuation aspects, offers the new insights and perspective for the driven-dissipation systems that would stimulate the research on novel properties of low-frequency vibrations of the materials far from equilibrium.

We gratefully acknowledge the support of Air Force Office of Research Grant No. FA-9550-18-1-0141, Office of Naval Research Grant No. N00014-16-1-3054, and Robert A. Welch Foundation (Grants No. A-1261 and No. A-1943-20180324). We also thank V. V. Yakovlev, K. Wang, Z. H. Yi, A. Sokolov, and M. King for the useful discussions.

*zhedong.zhang@tamu.edu
†girish.agarwal@tamu.edu
‡scully@tamu.edu

[1] J. Kasprzak *et al.*, Nature (London) **443**, 409 (2006).
[2] A. Amo, J. Lefrère, S. Pigeon, C. Adrados, C. Ciuti, I. Carusotto, R. Houdré, E. Giacobino, and A. Bramati, Nat. Phys. **5**, 805 (2009).
[3] M. Soriente, T. Donner, R. Chitra, and O. Zilberberg, Phys. Rev. Lett. **120**, 183603 (2018).
[4] G. S. Engel, T. R. Calhoun, E. L. Read, T.-K. Ahn, T. Mančal, Y.-C. Cheng, R. E. Blankenship, and G. R. Fleming, Nature (London) **446**, 782 (2007).
[5] Z. D. Zhang and J. Wang, Sci. Rep. **6**, 37629 (2016).
[6] A. Ishizaki and G. R. Fleming, Annu. Rev. Condens. Matter Phys. **3**, 333 (2012).
[7] Z. D. Zhang and J. Wang, J. Phys. Chem. B **119**, 4662 (2015).
[8] S. Hameroff, Phil. Trans. R. Soc. A **356**, 1869 (1998).
[9] S. Hagan, S. R. Hameroff, and J. A. Tuszynski, Phys. Rev. E **65**, 061901 (2002).
[10] H. Fröhlich, Int. J. Quantum Chem. **2**, 641 (1968).
[11] J. A. Tuszynski, R. Paul, R. Chatterjee, and S. R. Sreenivasan, Phys. Rev. A **30**, 2666 (1984).
[12] J. A. Tuszynski and J. M. Dixon, Phys. Rev. E **64**, 051915 (2001).
[13] J. Pokorny, J. Theor. Biol. **98**, 21 (1982).
[14] M. V. Mesquita, A. R. Vasconcellos, R. Luzzi, and S. Mascarenhas, Int. J. Quantum Chem. **102**, 1116 (2005).
[15] K. B. Davis, M. O. Mewes, M. R. Andrews, N. J. van Druten, D. S. Durfee, D. M. Kurn, and W. Ketterle, Phys. Rev. Lett. **75**, 3969 (1995).
[16] D. S. Jin, J. R. Ensher, M. R. Matthews, C. E. Wieman, and E. A. Cornell, Phys. Rev. Lett. **77**, 420 (1996).
[17] C. J. Pethick and H. Smith, *Bose-Einstein Condensation in Dilute Gases* (Cambridge University Press, Cambridge, United Kingdom, 2001).
[18] I. Altfeder, A. A. Voevodin, M. H. Check, S. M. Eichfeld, J. A. Robinson, and A. V. Balatsky, Sci. Rep. **7**, 43214 (2017). Here the phonon condensate has been observed in a monolayer of 2D material WSe_2. Unlike the Fröhlich condensate, this is at equilibrium because there is no external energy pumping added.
[19] M. O. Scully and W. E. Lamb, Jr., Phys. Rev. Lett. **16**, 853 (1966).
[20] M. O. Scully and W. E. Lamb, Jr., Phys. Rev. **159**, 208 (1967).
[21] M. O. Scully and W. E. Lamb, Jr., Phys. Rev. **166**, 246 (1968).
[22] M. O. Scully and W. E. Lamb, Jr., Phys. Rev. **179**, 368 (1969).

[23] M. O. Scully, Phys. Rev. Lett. **82**, 3927 (1999).
[24] T. M. Wu and S. J. Austin, J. Biol. Phys. **9**, 97 (1981).
[25] J. R. Reimers, L. K. McKemmish, R. H. McKenzie, A. E. Mark, and N. S. Hush, Proc. Natl. Acad. Sci. U.S.A. **106**, 4219 (2009).
[26] It may be noted that the redistribution of energy by the pumping mechanism could allow for the control of reaction kinetics. The energy distribution among vibrational modes of molecules is important in other contexts, such as the modification of chemical reactions referred to A. Thomas *et al.*, Angew. Chem., Int. Ed. **55**, 11462 (2016).
[27] V. DeGiorgio and M. O. Scully, Phys. Rev. A **2**, 1170 (1970).
[28] K. E. Dorfman, D. V. Voronine, S. Mukamel, and M. O. Scully, Proc. Natl. Acad. Sci. U.S.A. **110**, 2746 (2013).
[29] Z. D. Zhang and J. Wang, J. Chem. Phys. **140**, 245101 (2014).
[30] J. Miao, P. Charalambous, J. Kirz, and D. Sayre, Nature (London) **400**, 342 (1999).
[31] I. V. Lundholm, H. Rodilla, W. Y. Wahlgren, A. Duelli, G. Bourenkov, J. Vukusic, R. Friedman, J. Stake, T. Schneider, and G. Katona, Struct. Dyn. **2**, 054702 (2015).
[32] D. A. Turton, H. M. Senn, T. Harwood, A. J. Lapthorn, E. M. Ellis, and K. Wynne, Nat. Commun. **5**, 3999 (2014).
[33] I. Nardecchia *et al.*, Phys. Rev. X **8**, 031061 (2018).
[34] H. Haken, Rev. Mod. Phys. **47**, 67 (1975).
[35] Z. D. Zhang, K. Bennett, V. Chernyak, and S. Mukamel, J. Phys. Chem. Lett. **8**, 3387 (2017).
[36] D. A. Potoyan and P. G. Wolynes, Proc. Natl. Acad. Sci. U.S.A. **111**, 2391 (2014).
[37] C. H. Li and J. Wang, Proc. Natl. Acad. Sci. U.S.A. **111**, 14130 (2014).
[38] M. Klaas *et al.*, Phys. Rev. Lett. **121**, 047401 (2018).
[39] A. S. Dabydov, J. Theor. Biol. **38**, 559 (1973).
[40] G. S. Agarwal, *Quantum Optics* (Cambridge University Press, Cambridge, United Kingdom, 2013).
[41] M. O. Scully and S. Zubairy, *Quantum Optics* (Cambridge University Press, Cambridge, United Kingdom, 1997).
[42] See Supplemental Material at http://link.aps.org/supplemental/10.1103/PhysRevLett.122.158101 for math details, which includes Refs. [5,7,10,23,24,29,33,40, 41,43].
[43] C. N. Yang, Rev. Mod. Phys. **34**, 694 (1962).
[44] J. Pokorny, Bioelectrochem. Bioenerg. **63**, 321 (2004).
[45] S. Sahu, S. Ghosh, D. Fujita, and A. Bandyopadhyay, Sci. Rep. **4**, 7303 (2014).
[46] S. R. Hameroff, J. Conscious. Stud. **1**, 91 (1994).
[47] The longitudinal modes that are most electromagnetically active in MTs are expected to be in GHz regime [50,51] and these would require much higher pumping power, making the possibility of observing Fröhlich condensation in MTs somewhat remote.
[48] S.Ya. Tochitsky, C. Sung, S. E. Trubnick, C. Joshi, and K. L. Vodopyanov, J. Opt. Soc. Am. B **24**, 2509 (2007).
[49] D. R. Martin and D. V. Matyushov, J. Chem. Phys. **147**, 084502 (2017).
[50] X. S. Qian, J. Q. Zhang, and C. Q. Ru, J. Appl. Phys. **101**, 084702 (2007).
[51] J. Pokorny, C. Vedruccio, M. Cifra, and O. Kucera, Eur. Biophys. J. **40**, 747 (2011).